Thermal Science and Engineering Progress 17 (2020) 100378

Contents lists available at ScienceDirect

Thermal Science and Engineering Progress

journal homepage: www.elsevier.com/locate/tsep

# Numerical and experimental investigation of melting characteristics of phase change material-RT58

Ajay Kumar Yadav*, Teja Donepudi, Bhargav Sriram Siddani

*Department of Mechanical Engineering, National Institute of Technology Karnataka, Surathkal, Mangalore 575025, Karnataka, India*

ARTICLE INFO

*Keywords:*
Phase change material
RT-58
Melting and solidification
Heat transfer
Constrained and unconstrained melting
Computational fluid dynamics

ABSTRACT

The present study is focused on experimental and numerical analysis of unconstrained melting of Paraffin wax-RT58 in a horizontally placed cylindrical container. After the validation of numerical model with experimental results, numerical analysis is extended to constrained melting to investigate the process. The experiments are carried out at constant wall temperature maintained on the lateral surface of the cylinder. The influence of initial sub-cooling and lateral surface temperature on the melting rate is investigated. The melting process is better analyzed by the melting phase front and temperature contours as time progresses. The results show that the melting rate decreases by increasing the initial sub-cooling, and increases with increasing lateral surface temperature of the cylinder. In unconstrained melting, heat transfer by conduction governs the melting process initially, but later it is restricted to only the bottom part of the cylinder as the solid PCM at a higher density sinks due to effects of gravity. Heat transfer in the upper half of the cylinder is dominated by natural convection set up in the liquid PCM. In constrained melting, pure conduction phenomenon exists only in the beginning, and later conjugate heat transfer occurs. When subjected to similar boundary conditions, PCM melt-time is lower in unconstrained melting than in constrained melting. A correlation between melt-time and Stefan number is also developed.

## 1. Introduction

Latent heat storage is an efficient mode of storing thermal energy in which a material undergoes phase change. The use of Phase Change Material (PCM) for thermal energy storage has been a major area of research worldwide due to its ability to store/release large amount of heat during melting/solidification at approximately isothermal condition. As a consequence of their higher energy storage densities, they are used in numerous applications, Baby et al. [1] experimentally investigated their applications in finned heat sinks for electronic equipment cooling, Meng et al. [2] used a composite PCM as a thermal energy storage unit and studied their performance over varying operating conditions and a comprehensive review on selection criteria of PCMs for free cooling of buildings including various experimental and numerical simulations carried out by researchers was done by Thambidurai et al. [3]. The selection of appropriate PCM is based on working temperature range.

In solar thermal energy storage systems PCMs are typically placed in cylindrical tubes where heat is transferred to PCM by the hot working fluid coming out of the concentrator. Adine et al. [4] numerically studied the effect of using two PCMs in shell space against using a single PCM over a range of varying key parameters, the enhanced thermal conductivity of PCMs obtained upon adding carbon fibers and bushes was investigated both numerically and experimentally by Hamada et al. [5] and a finite difference approach to study the transient phase change thermal storage system of vertical tube type for varying Reynold and Stefan numbers was done by Ismail et al. [6].

Melting of PCM in a container is of two types: constrained and unconstrained. Solid PCM is restricted from sinking in case of constrained melting but sinks in unconstrained melting due to gravity, this is schematically represented in Fig. 1. Melting in cylindrical containers has been studied extensively in the past. Shamsundar and Sparrow [7] studied unconstrained melting in circular tubes but assumed conduction to be the only mode of heat transfer, while Rieger et al. [8] and Ho and Viskanta [9] assumed constrained melting process in which solid PCM is supported at the center. Bareiss and Beer [10] investigated the effect of natural convection on melting process in vertical cylindrical arrangement with variable height. Later experimental and analytical solution determining the heat transfer coefficients and melting rates were performed by them [11] on a range of PCMs for different operating parameters, considering many simplifying assumptions made in the previous studies, and developed a non-dimensional expression for

* Corresponding author.
*E-mail address:* ajaykyadav@nitk.edu.in (A.K. Yadav).

https://doi.org/10.1016/j.tsep.2019.100378
Received 2 February 2019; Received in revised form 6 July 2019; Accepted 7 July 2019

**Nomenclature**

| | |
|---|---|
| $Ac$ | Area of cross-section of container, $m^2$ |
| $A_s$ | Area of cross-section of solid PCM, $m^2$ |
| $C$ | Mushy Zone Constant, $kgm^{-3}s^{-1}$ |
| $c_p$ | Specific heat, $Jkg^{-1}$ |
| $D$ | Diameter, mm |
| $g$ | Acceleration due to gravity, $ms^{-2}$ |
| $h_s$ | Sensible heat, $Jkg^{-1}$ |
| H | Enthalpy, $Jkg^{-1}$ |
| $h_{ref}$ | Reference Enthalpy, $Jkg^{-1}$ |
| $h_s$ | Sensible Heat, $Jkg^{-1}$ |
| $k$ | Thermal conductivity, $Wm^{-1}K^{-1}$ |
| $L$ | Latent heat, $Jkg^{-1}$ |
| $P$ | Pressure, Pa |
| $t$ | Time, s |
| $T$ | Temperature, K |
| $T_i$ | Initial Temperature, K |
| $T_{liquidus}$ | Liquid PCM temperature, K |
| $T_m$ | Melting Temperature, K |
| $T_{pcm}$ | Temperature of PCM, K |
| $T_{solidus}$ | Solid PCM temperature, K |
| $T_w$ | Wall Temperature, K |
| Ste | Stefan number |
| $V$ | Velocity, $ms^{-1}$ |

*Greek symbols*

| | |
|---|---|
| β | Liquid fraction |
| ρ | Density, $kgm^{-3}$ |
| $\mu$ | Dynamic viscosity, $kgm^{-1}s^{-1}$ |
| $\alpha$ | Thermal diffusivity, $m^2s^{-1}$ |
| $\tau$ | Non-dimensional time |
| ε | Computational Constant |

melt-time of PCM which is initially at its melting point.

Prasad and Sengupta [12] obtained comprehensive numerical solution to the problem by making use of some results from Ho and Viskanta [9] over a wide range of Rayleigh numbers. They concluded that Nusselt number along the upper wall and upper solid-liquid interface region increases with increasing Rayleigh number, implying higher rates of heat transfer. At the bottom, solid PCM and the wall are separated by a thin film of liquid, resulting in large heat fluxes due to high temperature gradients causing higher melting at the bottom than in the upper half where natural convection cells are set-up in the liquid PCM.

Roy and Sengupta [13] developed a family of curves for analyzing contact melting in spherical enclosures which were experimentally validated by Moore and Bayazitgolu [14] using n-octadecane. Prasad and Sengupta [15] extended their previous work [13] by varying Rayleigh, Prandtl and Stefan numbers in the range of solar thermal energy storage systems, and by performing multiple regression analysis they developed correlations for mean heat flux on the upper wall of cylinder as well as interface at the symmetry point and melt time of the solid. Melt-time relation for contact melting in spherical capsule was also developed by Brahmi and Wang [16]. A single correlation for contact melting in various geometrical configurations was given by Bejan [17] by performing scaling analysis.

Melting characteristics of n-octadecane for both constrained and unconstrained cases inside a spherical capsule was experimentally studied by Tan [18]. Later Sattari et al. [19] performed a 2-dimensional numerical analysis of Tan [18] constrained melting process by reducing the sphere to a 2-dimensional circular domain with an elevated wall temperature along the circumference and studied the influence of wall temperature, initial sub-cooling and size of the capsule on melt rate. But reducing sphere to a 2-dimensional circle ignores the varying cross-sectional area of a sphere, and heat transfer is assumed only along the radial direction without taking into account the axial direction. A correct experimental setup of the computational domain (2-D circle) would be a horizontal cylinder with its lateral surfaces at an elevated temperature.

In the present study, numerical simulation of unconstrained melting of RT-58 in a circular domain is performed using ANSYS-Fluent software. After validating with experimental results, the numerical analysis has been extended to constrained melting. The effect PCM initial temperature and Stefan number has been studied. A non-dimensional relation between melt-time and Stefan number has been developed that would save both experimental costs and computational time of numerical analysis to determine the time in which PCM completely melts

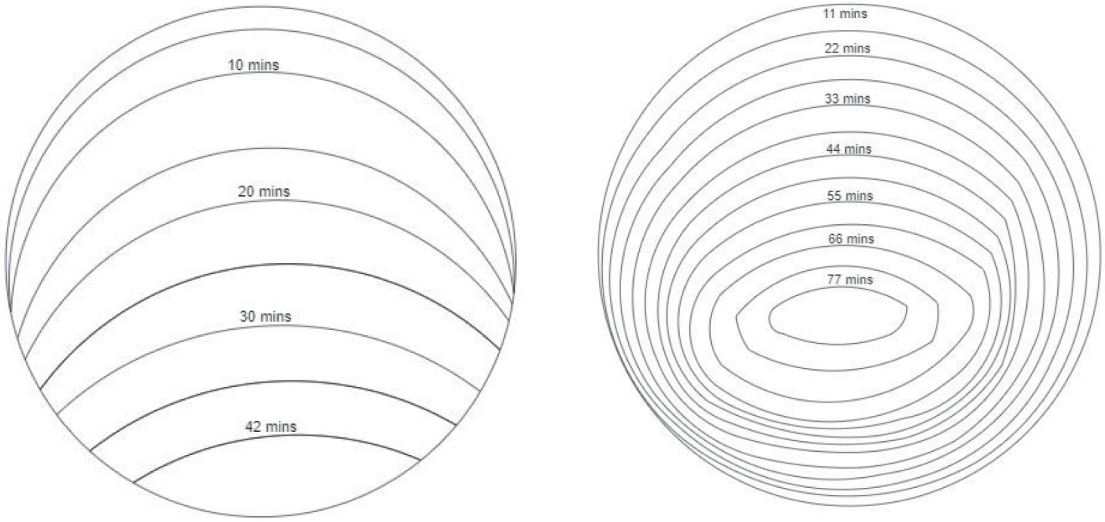


**Fig. 1.** Schematic representation constrained and unconstrained melting.

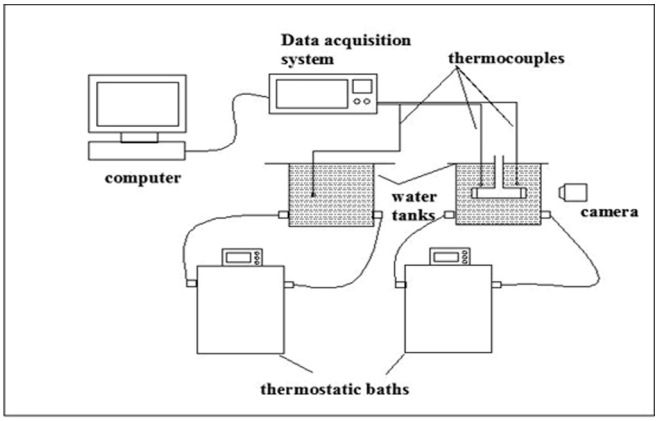


**Fig. 2.** Schematic of the experimental setup.

absorbing energy for a given wall/external temperature.

## 2. Experimental setup

The experimental setup for unconstrained melting is shown in Fig. 2. The setup consists of two water tanks, a cylindrical container, K-type thermocouples, two thermostatic baths, a data acquisition unit, inlet and exhaust valves. Each of the water tanks is connected to respective thermostatic baths (Make: Siskin Instruments; Model: Thermo scientific PC200) having a heating/cooling capacity of 2 kW which provide water at constant temperature with an accuracy of ± 0.01 °C. The flow rate of water is controlled using inlet and exhaust valves. A computer integrated data acquisition system (Keithley – Model 2700) is employed to record temperatures from various thermocouples during the experiments with the accuracy of ± 0.01 °C.

Sub-cooling temperature ($\Delta T$) is defined as $\Delta T = T_m - T_i$. Initial sub-cooling of PCM is achieved in one of the tanks and sensible heating takes place in the other. As soon as the PCM reaches the desired initial sub-cooling temperature, it is transferred to other tank in which water is at elevated temperature. The glass temperature is continuously monitored using thermocouples placed along its lateral surface.

The storage unit is of outer diameter 58 mm and internal volume of 250 ml as shown in Fig. 3. In order to provide isothermal conditions only along the lateral surface, two glass caps, which act as an insulation are glued to the end faces.

The PCM RT-58 is used for study and its thermophysical properties are given in Table 1. The storage unit is made of glass having 1.5 mm thickness and thermal conductivity of 1.15 $Wm^{-1}K^{-1}$.

**Table 1**
Thermophysical properties of RT-58.

| Properties | Value |
|---|---|
| Melting temperature | 55–60 °C |
| Density | 850 $kgm^{-3}$ (solid)<br>775 $kgm^{-3}$ (liquid) |
| Kinematic viscosity | $3.165 \times 10^{-5}\ m^2s^{-1}$ |
| Specific heat | 900 $Jkg^{-1}K^{-1}$ |
| Thermal conductivity | 0.2 $Wm^{-1}k^{-1}$ |
| Latent heat of fusion | 230 k $Jkg^{-1}$ |
| Thermal expansion coefficient | 0.000764 $K^{-1}$ |

## 3. Numerical model

The numerical calculations were carried out using FLUENT-14.5 software. A 2-dimensional cross-section of the cylinder is chosen for the analysis. At the start, it is completely filled with solid PCM at a temperature ($T_i$) lower than its melting temperature ($T_m$). It is then subjected to an elevated temperature $T_w$, ($T_w > T_m$) along the circumference.

Melting process is assumed to be 2-dimensional, unsteady, incompressible and laminar. Solid and liquid phases are assumed to be homogeneous, isotropic and in thermal equilibrium.

For the mushy zone, enthalpy-porosity approach [20] is used, in which the porosity in each cell is equal to the liquid fraction in that cell. The governing equations solved numerically are given below.

Continuity-

$$\frac{\partial \rho}{\partial t} + \nabla.(\rho V) = 0 \tag{1}$$

Momentum-

$$\frac{\partial(\rho\vec{V})}{\partial t} + \nabla.(\rho\vec{V}) = -\nabla P + \mu\nabla^2\vec{V} + \rho\vec{g} + \vec{S} \tag{2}$$

Energy-

$$\frac{\partial(\rho H)}{\partial t} + \nabla.(\rho V H) = \nabla.(k\nabla T_{pcm}) \tag{3}$$

Here $H$ is enthalpy of the material and is given by

$$H = h_s + \Delta H \tag{4}$$

where $h_s$ is the sensible heat and $\Delta H$ is the latent heat of the material. They are calculated using

$$h_s = h_{ref} + \int_{T_{ref}}^{T_{pcm}} c_p dT \tag{5}$$

The value of $\Delta H$ depends on the liquid fraction β, and is given by

$$\Delta H = \beta L \tag{6}$$

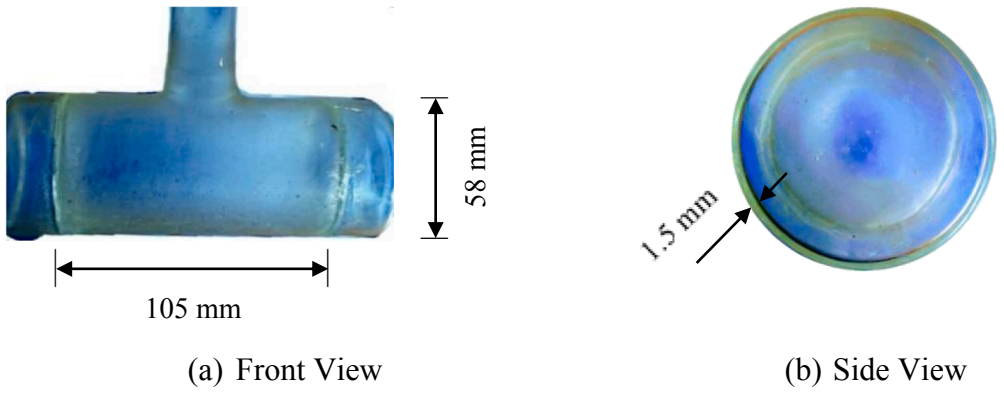


**Fig. 3.** Storage unit along with dimensions.

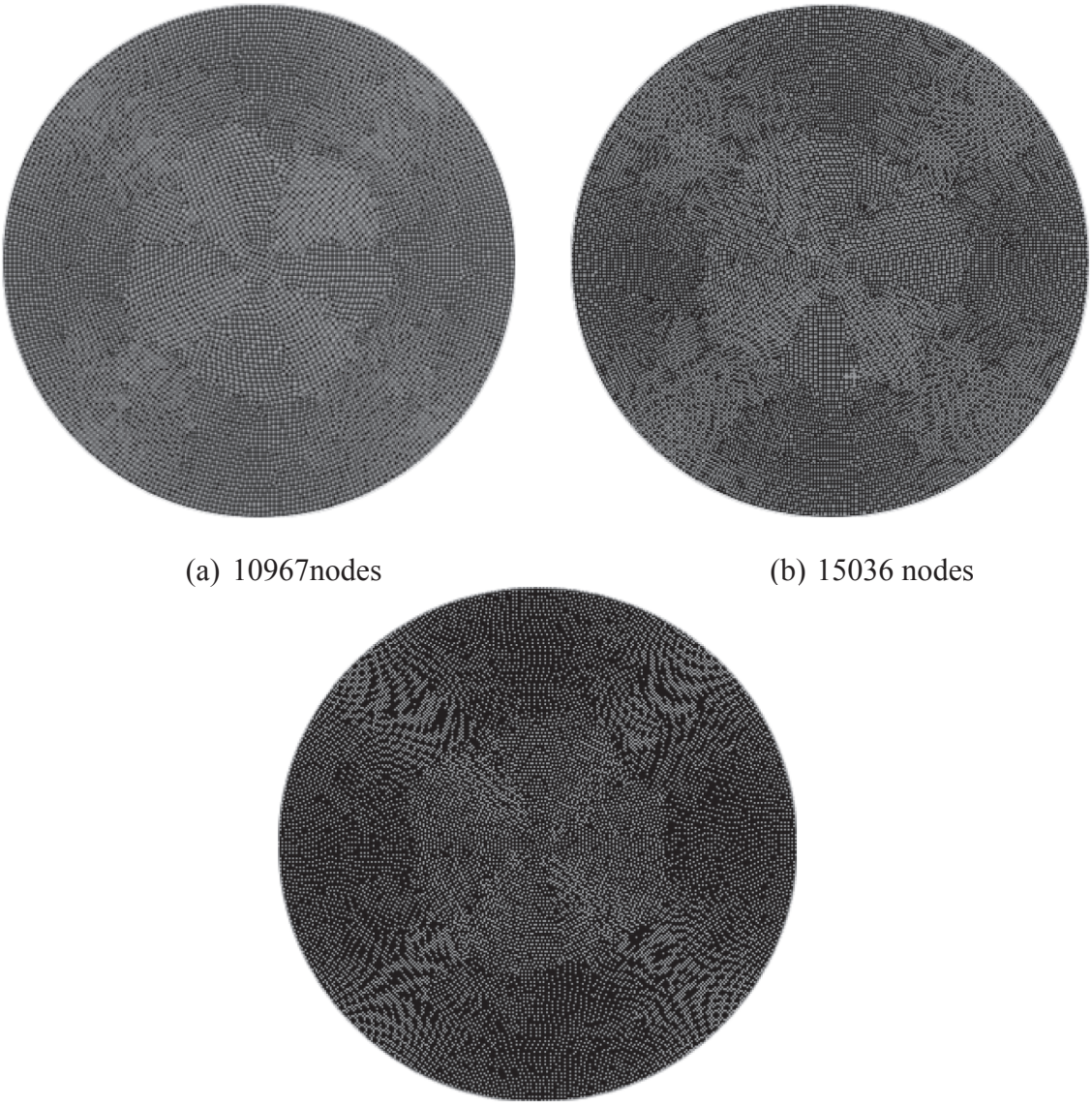


**Fig. 4.** Meshing of computational domain.

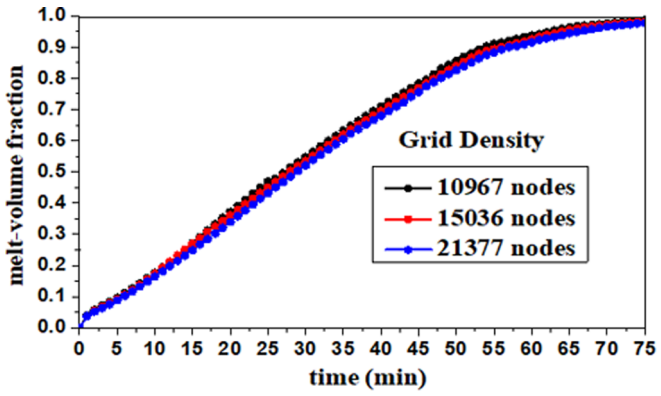


**Fig. 5.** Melt-volume fractions v/s time at varying grid densities.

where

$$\begin{aligned} \beta &= 0 && if\ T_{pcm} < T_{solidus} \\ \beta &= 1 && if\ T_{pcm} > T_{solidus} \\ \beta &= \frac{T - T_{solidus}}{T_{liquidus} - T_{solidus}} && if\ T_{solidus} < T_{pcm} < T_{liquidus} \end{aligned} \tag{7}$$

The source term $\vec{S}$ is given by:

$$\vec{S} = \frac{C(1-\beta)^2}{(\beta^3 + \varepsilon)}(\vec{v} - \overrightarrow{v_p}) \tag{8}$$

where ε = 0.001 is a small computational constant used to avoid division by zero, $\overrightarrow{v_p}$ is the pull velocity of solid which reduces to zero in case of constrained melting, and $C$ is the mushy zone constant. An increase in its value reduces flow in mushy zone i.e. higher the value, sharper is

the transition of velocity of the material as it solidifies; its value is set to $10^5$ in the present study and shows excellent agreement with experimental results obtained as shown in Fig. 7.

Pressure and velocity coupling is done using SIMPLE (semi-implicit method for pressure-linked equations) algorithm. As the study includes convection and curved domain, PRESTO (Pressure Staggering Options) scheme is employed. The momentum and energy equations are discretized using power law scheme.

A fine quadrilateral mesh along the radial direction is adopted as shown in Fig. 4.

In order to prove grid-independent convergence, different grid densities were adopted as shown in Fig. 5, and the time taken to melt the PCM is chosen as the governing parameter. The effect of time step was also examined for 0.01, 0.1 and 0.5 s. As a result, 15,036 nodes with a time step size of 0.1 s were found to be sufficient.

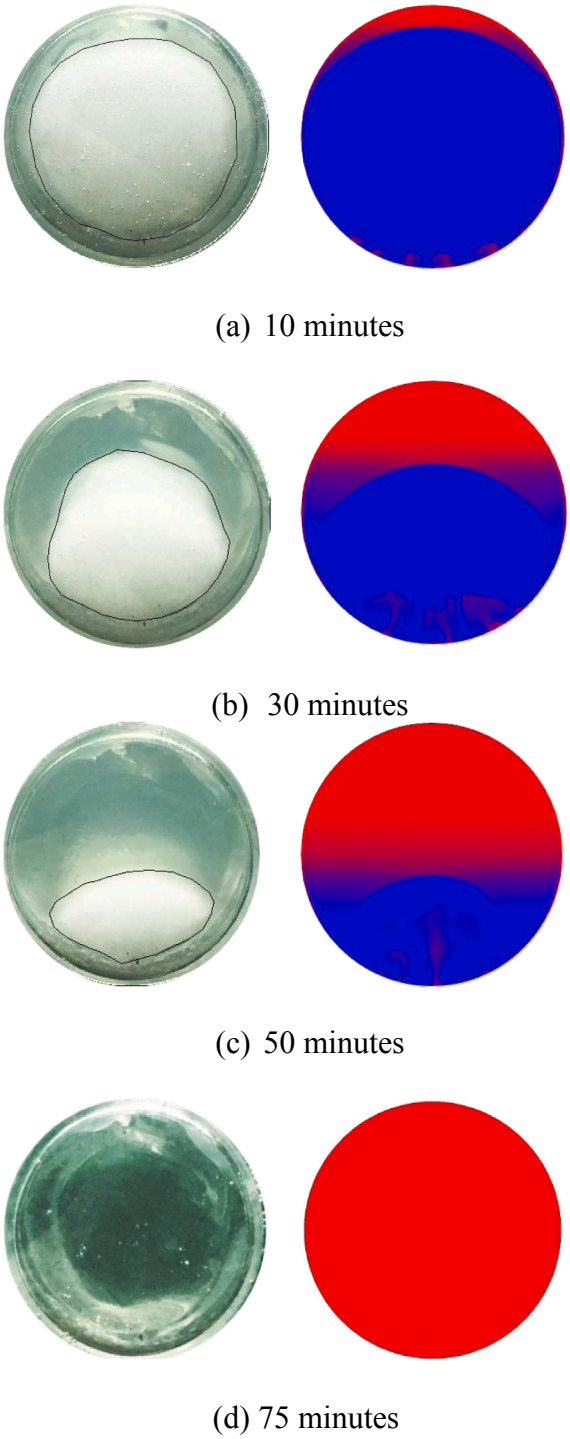


**Fig. 6.** Melt phase fronts at Ste = 0.0235 and initial sub-cooling of 25 °C.

## 4. Results and discussion

Stefan number (Ste) is an important parameter in melting and solidification which is defined as the ratio of sensible heat to latent heat of PCM, and is directly proportional to wall temperature,

$$Ste = \frac{C_P(T_w - T_m)}{L} \tag{9}$$

### 4.1. Validation of numerical model

Melting process of the PCM is investigated experimentally at a wall temperature of 61 °C (Ste = 0.0235) and sub-cooling of 25 °C. Digital images of the melt phase front are captured at regular intervals as shown in Fig. 6, solid PCM is enclosed within the black boundary as shown. The total melt-time of the PCM is 75 min at the experimental conditions mentioned.

Initially, conduction is the only mode of heat transfer taking place between the inner surface of the container and solid PCM. Gradually, PCM melts along the lateral surface, liquid PCM begins to rise up sinking the solid PCM due to higher density as can be seen from Fig. 6(b). Conduction is still dominant in the bottom half of the container where solid PCM is always in contact with the container. The thickness of liquid PCM of lower density occupying the top half increases, resulting in convective heat transfer between the solid and liquid phases. Along the lateral surface a very thin layer of molten PCM exists, although it is not possible to detect it photographically. In Fig. 6(c), natural convection is setup in the liquid PCM where cooler liquid is continuously replaced by the warmer liquid PCM flowing inwards. An oval shaped profile is formed throughout the experiment, which shows higher rate of melting in the conduction dominated zone i.e., bottom half. The volume fraction contours obtained by numerical analysis are also shown. The blue and red zones represent complete solid and liquid zones respectively. In order to validate the results, melt-volume fraction obtained from numerical and experimental studies are compared. To obtain the melt-volume fraction of the experimental study, digital images are uploaded into CAD modeling software and the solid-liquid phase fronts are captured. The melt-volume fraction ($f$) can be obtained by using

$$f = 1 - \frac{A_s}{A_c} \tag{10}$$

where $A_s$ and $A_c$ represent the area of solid PCM and container

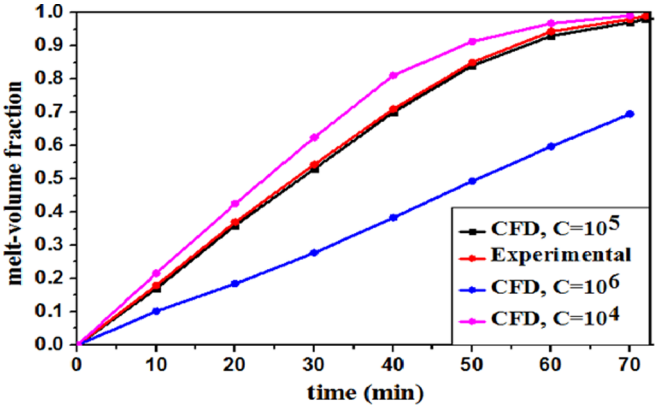


**Fig. 7.** Variation of melt volume fraction with mushy constant at Ste = 0.0235 and sub-cooling of 25 °C.

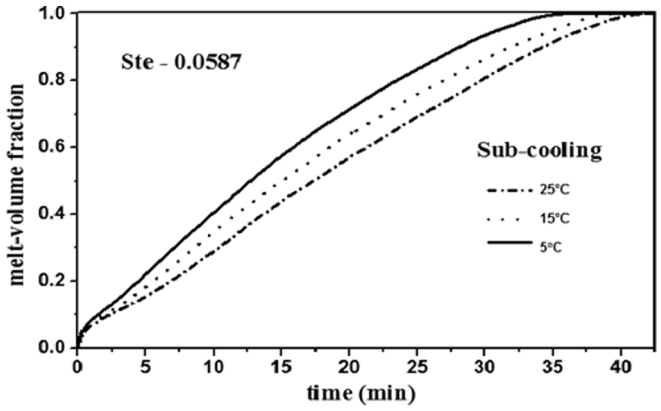


**Fig. 8.** Variation of melt-volume fraction with initial sub-cooling at Ste = 0.0587.

respectively.

#### 4.1.1. Determining mushy constant for present study

Mushy Zone Constant C is the damping term in the momentum equation in order to model fluid flow in solid/liquid interface fluid flow through porous medium. The effect of mushy constant C on the melt-volume fraction was studied as shown in Fig. 7. As mushy zone constant is increased the melt time increases as overall heat transfer rate decreases with bouncy driven currents being forced to zero due to greater influence of mushy zone constant. Thermohydraulics of a PCM is significantly affected by the value of Mushy Zone Constant and hence its optimal value of it must be determined for numerical analysis by comparing melt volume fraction as time progresses. A good agreement with experimental results was obtained at $C = 10^5$.

### 4.2. Effect of Sub-cooling on melt volume fraction

Fig. 8 shows the variation of melt-volume fraction with initial PCM temperature at Ste = 0.0587. As can be seen from the graph, melting rate increases with decrease in initial sub-cooling. The melt-time decreases rapidly at lower sub-cooling, it drops by 9.3% by decreasing sub-cooling from 15 °C to 5 °C (66.7% decrease), while a marginal decrease of 5.8% in melt-time is obtained by raising the sub-cooling temperature from 15 °C to 25 °C (66.7% rise).

### 4.3. Effect of Stefan number on melt volume fraction

The melting rates at an initial sub-cooling of 5 °C is shown in Fig. 9, for 34.5% increase in Stefan number (0.058–0.078), total-melt time

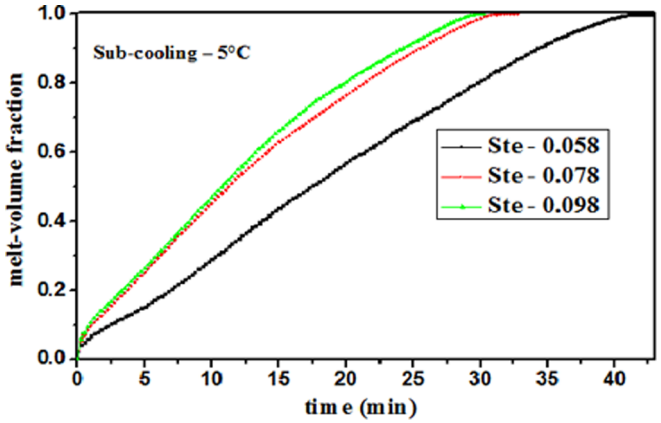


**Fig. 9.** Variation of melt-volume fraction with Stefan number at sub-cooling of 5 °C.

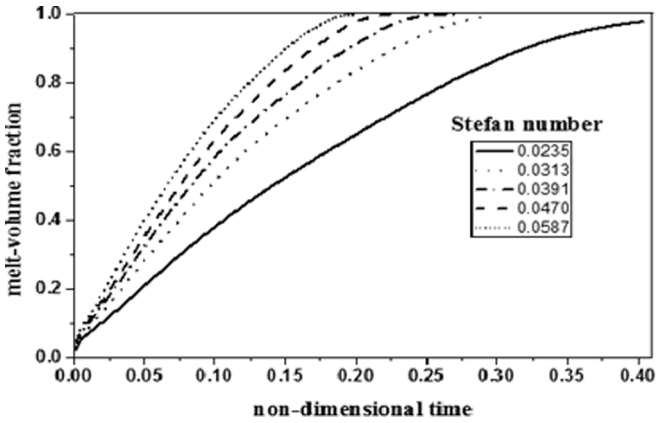


**Fig. 10.** Variation of melt-volume fraction with Stefan number with pcm initially at melting temperature.

**Table 2**
Non-dimensional melt time for varying Stefan numbers.

| Stefan number | Actual melt time | Melt time from correlation |
|---|---|---|
| 0.024 | 0.404 | 0.389 |
| 0.031 | 0.294 | 0.313 |
| 0.039 | 0.275 | 0.265 |
| 0.047 | 0.225 | 0.230 |
| 0.058 | 0.201 | 0.197 |

reduction of 20.3% is observed, and a little variation is observed for Stefan numbers above 0.098. The increase in melt-rate with increasing Stefan number can be attributed to increased heat transfer though the wall to the PCM.

### 4.4. Melt time correlation

Non-dimensional time ($\tau$) is defined as

$$\tau = t \times \left(\frac{\alpha}{D^2}\right) \tag{11}$$

where α is the thermal diffusivity of the PCM and $D$ is the diameter of the container.

The variation of melt-volume fraction with non-dimensional time at varying Stefan numbers is shown in Fig. 10, in which the PCM is assumed to be at melting temperature ($T_m$) initially. Results show that melt time decreases with increasing Stefan number as discussed earlier.

A correlation between non-dimensional time and Stefan number is

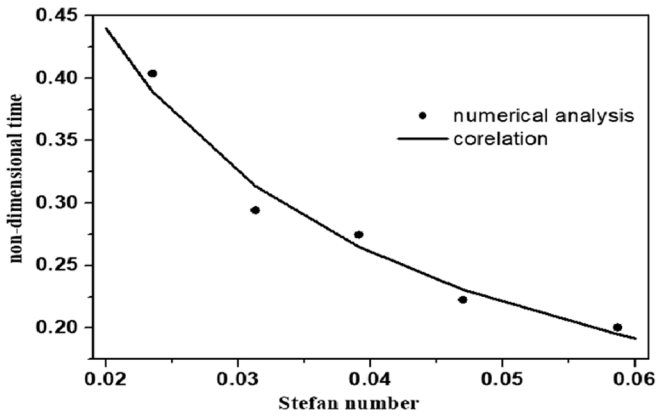


**Fig. 11.** Melt time obtained by numerical analysis and correlation.

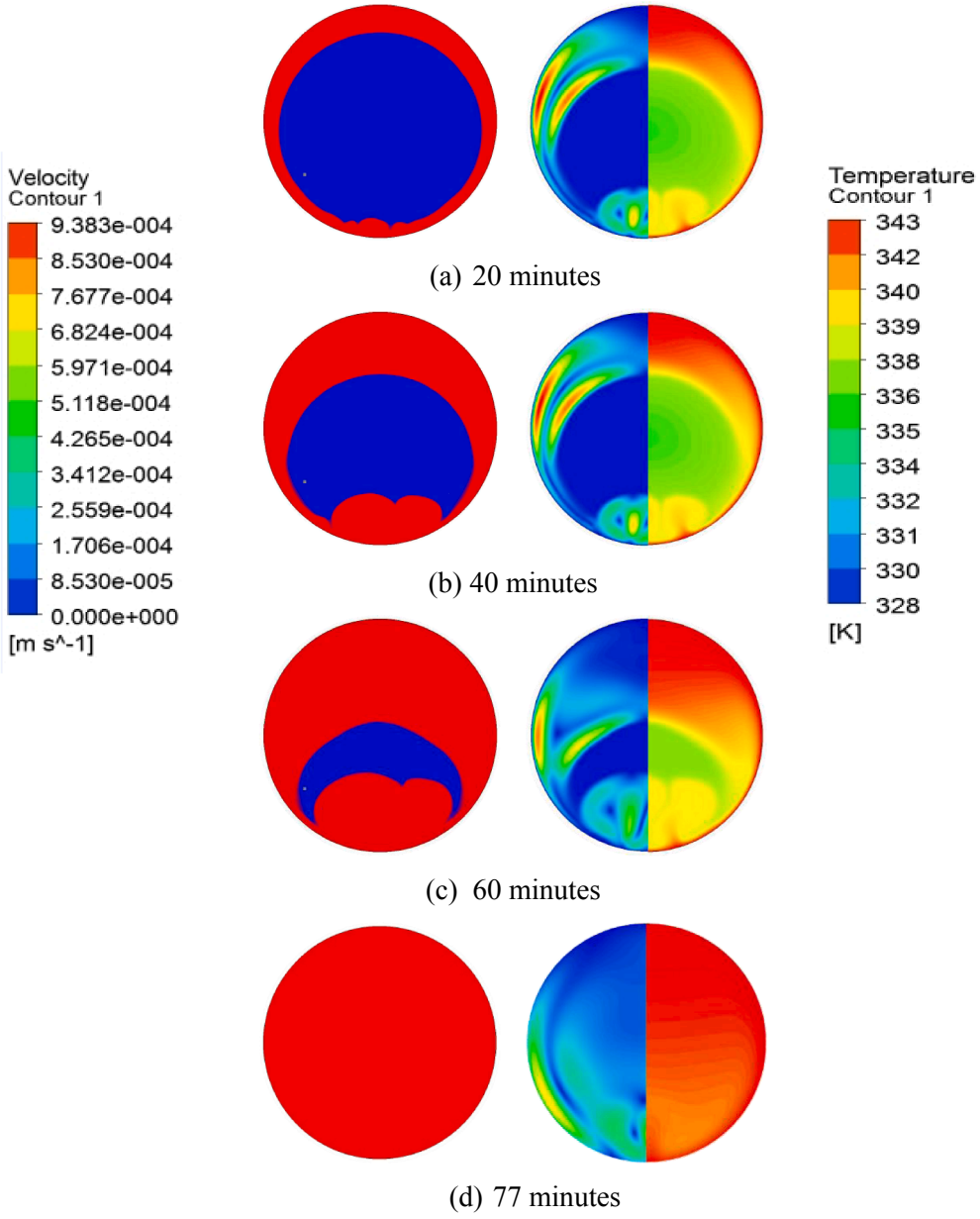


**Fig. 12.** Melt phase fronts (left), velocity and temperature contours (right) at Ste- 0.0235 and sub-cooling of 25 °C.

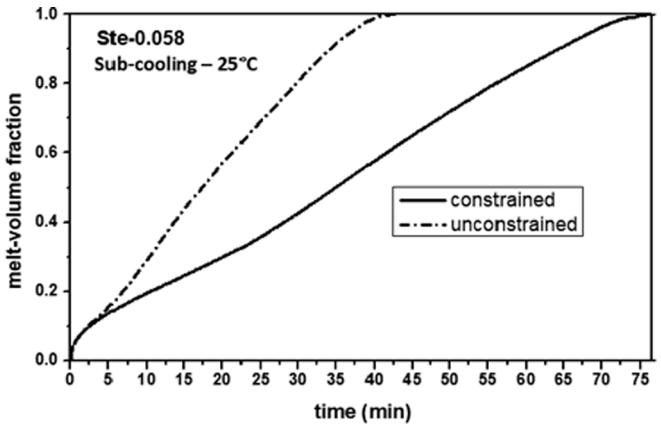


**Fig. 13.** Melt volume fraction vs time for constrained and unconstrained melting at Ste = 0.058, and sub-cooling of 25 °C.

developed using linear regression analysis.

$$\tau = 0.0229 \times Ste^{-0.755} \tag{12}$$

This equation is valid for Stefan numbers between 0.02 and 0.06. Regression coefficient, $R^2$ is used as a statistical measure to determine the functional relationship between two or more variables (non-dimensional melt-time and Stefan number in this case). It is calculated using the formula

$$R^2 = \frac{\Sigma\left(\hat{\tau} - \bar{\tau}\right)^2}{\Sigma\left(\tau - \bar{\tau}\right)^2} \tag{13}$$

where $\hat{\tau}$ is the melt time obtained by obtained correlation (12), $\bar{\tau}$ is the average melt time over the Stefan number range and $\tau$is the actual melt time of PCM. The obtained correlation has a $R^2$ value of 97.1%. Table 2 shows the non-dimensional melt time obtained by correlation and

actual melt time for varying Stefan numbers and Fig. 11 is a graphical representation of the same.

### 4.5. Constrained melting

Fig. 12 shows volume fraction contours of constrained melting process obtained from numerical simulations at a Stefan number of 0.058 and initial sub-cooling of 25 °C. Contours of temperature and velocity are also shown in Fig. 12, on the right and left half planes respectively. It is observed that the melt phase front is initially concentric as seen from Fig. 12(a), where conduction between the solid PCM and inner wall of the cylinder is the dominant mode of heat transfer. As time progresses, rate of melting is higher in the top half as shown in Fig. 12(b) due to influence of natural convection as the warm liquid PCM rises up replacing the cooler liquid forming an oval shaped profile in that zone. Fig. 12(c) shows a wavy profile at the bottom half, which can be attributed to increasing influence of natural convection as liquid layer grows in the bottom half. Since heat transfer rate is less in this case, total melt time is higher i.e., 77 min against 43 min in unconstrained melting at the same conditions.

Fig. 13 shows a comparison graph of melt-volume fraction against time for constrained and unconstrained melting. The rate of melting is higher in unconstrained melting due to increased heat transfer rate by conduction heat transfer taking place in the bottom half of the container.

### 4.6. Error analysis

Minimum temperature measured during the experiments is 30 °C (melting point (55 °C)–subcooling (25 °C)) and least count of DAQ as well as thermostatic bath is ± 0.01 °C. Maximum fluctuation observed during the experiment to maintain the constant temperature of the tank is 0.5 °C. Hence, the maximum uncertainty in the case of temperature measurement is

$$\frac{\Delta T}{T} = \frac{\pm 0.5}{30} = \pm 0.0166 = \pm 1.66\%$$

## 5. Conclusion

The unconstrained melting process of RT-58 has been investigated both experimentally and numerically. Heat transfer process is dominated by conduction initially, but as time progresses liquid PCM formed is forced up and solid PCM sinks down simultaneously due to density differences. Conduction takes place only in the bottom half between the glass surface and solid PCM, and melting rate is higher in the bottom half as compared to the top half. Wall temperature has profound effect on melt-time as compared to the effects of sub-cooling. The melt-time correlation as function of Stefan number can be directly used to find the melt-time for various applications of thermal energy storage.

Further, the constrained melting process was studied numerically. Here conduction exists only in the beginning, later a thin layer of liquid PCM forms along the inner surface and conjugate heat transfer takes place. Natural convection cells are setup in the top half and melt faster as compared to the bottom half where a wavy profile is obtained.

The rate of heat transfer is higher in unconstrained melting as compared to constrained melting. Melting is higher in the bottom half in constrained melting due to conduction while top half melts faster in unconstrained melting due to natural convection in the liquid PCM. Melt-time is 44.2% lower in unconstrained melting at the same conditions.

## Declaration of Competing Interest

All authors declare that there is no conflict of interest.

## Acknowledgment

The present work was carried out under the department fund of Mechanical Engineering, NITK Surathkal, India. The financial support provided by the Mechanical Engineering department is gratefully acknowledged.

## Appendix A. Supplementary data

Supplementary data to this article can be found online at https://doi.org/10.1016/j.tsep.2019.100378.

## References

[1] R. Baby, C. Balaji, Experimental investigations on phase change material based finned heat sinks for electronic equipment cooling, Int. J. Heat Mass Transf. 55 (2012) 1642–1649.
[2] Z. Meng, P. Zhang, Experimental and numerical investigation of a tube-in-tank latent thermal energy storage unit using composite PCM, Appl. Energy 190 (2017) 524–539.
[3] M. Thambidurai, K. Panchabikesan, Krishna MohanN, V. Ramalingam, Review on phase change material based free cooling of buildings-the way toward sustainability, J. Energy Storage 4 (2015) 74–88.
[4] H.A. Adine, H.E. Qarnia, Numerical analysis of the thermal behaviour of a shell-and-tube heat storage unit using phase change materials, Appl. Math. Model. 33 (2009) 2132–2144.
[5] Y. Hamada, W. Ohtsu, J. Fukai, Thermal response in thermal energy storage material around heat transfer tubes: effect of additives on heat transfer rates, Sol. Energy 75 (2003) 317–328.
[6] K.A. Ismail, M.M. Abugderah, Performance of a thermal storage system of the vertical tube type, Energy Convers. Manage. 41 (2000) 1165–1190.
[7] N. Shamsundar, E.M. Sparrow, Storage of thermal energy by solid-liquid phase change-temperature drop and heat flux, J. Heat Transf. 96 (1974) 541.
[8] H. Rieger, U. Projahn, M. Bareiss, H. Beer, Heat transfer during melting inside a horizontal tube, J. Heat Transf. 105 (1983) 226.
[9] C. Ho, R. Viskanta, Heat transfer during inward melting in a horizontal tube, Int. J. Heat Mass Transf. 27 (1984) 705–716.
[10] M. Bareiss, H. Beer, Influence of natural convection on the melting process in a vertical cylindrical enclosure, Lett. Heat Mass Transf. 7 (1980) 329–338.
[11] M. Bareiss, H. Beer, An analytical solution of the heat transfer process during melting of an unfixed solid phase change material inside a horizontal tube, Int. J. Heat Mass Transf. 27 (1984) 739–746.
[12] A. Prasad, S. Sengupta, Numerical investigation of melting inside a horizontal cylinder including the effects of natural convection, J. Heat Transf. 109 (1987) 803.
[13] S.K. Roy, S. Sengupta, The melting process within spherical enclosures, J. Heat Transf. 109 (1987) 460.
[14] F.E. Moore, Y. Bayazitoglu, Melting within a spherical enclosure, J. Heat Transf. 104 (1982) 19.
[15] A. Prasad, S. Sengupta, Nusselt number and melt time correlations for melting inside a horizontal cylinder subjected to an isothermal wall temperature condition, J. Sol. Energy Eng. 110 (1988) 340.
[16] P.A. Bahrami, T.G. Wang, Gravity and conduction driven melting in a sphere, MRS Proc. 87 (1986).
[17] A. Bejan, Single correlation for theoretical contact melting results in various geometries, Int. Commun. Heat Mass Transf. 19 (1992) 473–483.
[18] F. Tan, Constrained and unconstrained melting inside a sphere, Int. Commun. Heat Mass Trans. 35 (2008) 466–475.
[19] H. Sattari, A. Mohebbi, M. Afsahi, A.A. Yancheshme, CFD simulation of melting process of phase change materials (PCMs) in a spherical capsule, Int. J. Refrig. 73 (2017) 209–218.
[20] V. Voller, C. Prakash, A fixed grid numerical modelling methodology for convection-diffusion mushy region phase-change problems, Int. J. Heat Mass Transf. 30 (1987) 1709–1719.